Editors' Suggestion

Polaronic interacceptor hopping transport in intrinsically doped nickel oxide

Robert Karsthof* and Marius Grundmann
Felix Bloch Institute for Solid State Physics, Universität Leipzig, Linnéstraße 5, 04103 Leipzig, Germany

Arthur Markus Anton and Friedrich Kremer
Peter Debye Institute for Soft Matter Physics, Universität Leipzig, Linnéstraße 5, 04103 Leipzig, Germany

(Received 12 April 2019; revised manuscript received 24 May 2019; published 20 June 2019)

In this work, we revisit the issue of the nature of electronic transport in nickel oxide (NiO) and show that the widely used model of free small polaron hopping, initially raised to characterize transport in high-purity samples, is not appropriate for modeling intrinsically doped NiO. Instead, we present extensive evidence, collected by means of temperature- and frequency-dependent measurements of the electrical conductivity σ, that the model of polaronic interacceptor hopping can be used to consistently explain the electronic conduction process. In this framework, holes are localized to acceptors (Ni vacancies), forming a strongly bound, polaron-like state. They can only move through the film by hopping to a neighboring, at least partially unoccupied, acceptor. This renders the spatial overlap between neighboring polaronic wave functions a highly critical parameter. The signature of this process is the occurrence of two temperature regions of the dc conductivity, separated by about half the Debye temperature $\frac{\theta_D}{2} \approx 200\,\mathrm{K}$. For $T > \frac{\theta_D}{2}$, holes are transferred by phonon-assisted hopping over the potential barrier between two sites, whereas phonon-assisted tunneling through the barrier dominates below that temperature. We also show that the degree of structural and electronic disorder plays a vital role in determining the characteristics of the transport process: high disorder leads to strong energetic broadening of the acceptor states such that hopping to more distant sites may be favored over transfer to nearest neighbors (variable range hopping). The assumption of high binding energies of the charge carriers at V_{Ni} is in accordance with the recent paradigm shift regarding the understanding of the electronic structure of NiO: holes doped into NiO couple to Ni 3*d* spins, thereby occupying deep polaron-like states within the band gap (Zhang-Rice bound doublets). This work explicitly takes this perception into account to explain carrier transport in NiO.

DOI: 10.1103/PhysRevB.99.235201

I. INTRODUCTION

The long-standing question on the origin of the dc conduction mechanism in nickel oxide has never been entirely settled. There exist numerous studies regarding this subject, many of which support the picture of polaronic conduction [1–7]; i.e., the hole is surrounded by a self-induced lattice distortion. Depending on the size of this distortion, the charge carrier can move by thermally activated hopping (for small polarons) or by conduction in a narrow band (mostly for large polarons when spatial overlap of the wave functions is appreciable). Evidence for both models has been presented in the literature. Austin and Mott have conjectured that the true value for the spatial extent r_p of the polaronic wave function lies somewhere between the "small" and "large" case [5]. This view has also been taken by Adler and Feinleib [7], based on an estimate of r_p on the order of two lattice spacings. On the other hand, ac studies have shown that *bound* charge carriers have probably small polaron character [8–11]. An entirely different picture has been proposed by Lunkenheimer *et al.*, who have interpreted their ac conductivity data within the framework of the *correlated barrier hopping* model [12]. In this model, the charge carriers are thought to hop from one acceptor site to another, with the hopping energy critically depending on the acceptor density [13], resembling the so-called impurity conduction in the hopping regime. In fact, there are several scientific publications from the 1960s conjecturing about the dc transport mechanism in NiO being due to interacceptor (or impurity) hopping conduction [5,6,9,10,14,15]. However, this view seems to have been abandoned later on in favor of "free" small or large polarons that can be transferred by hopping to any (sub)lattice site. To our view, this was mainly the result of an increased availability of low-impurity NiO samples at that time with considerably higher charge carrier mobilities than before. This demanded an alternative conduction model. In recent decades, researchers have aimed to use NiO in different (opto)electronic devices, which in many cases requires the material to be at least moderately conductive. To this end, doping (intrinsically or extrinsically) is often a prerequisite that should bring the impurity (or more generally, acceptor) hopping conduction model into focus again.

The perception of the hole in NiO was fundamentally changed in 1994 when Bała, Oleś, and Zaanen [16] applied a theory to NiO that was originally developed for high-T_c superconductors by Zhang and Rice [17]. It considers the coupling of the spin of a hole (introduced either by doping or by excitation) to the majority 3*d* spins at a neighboring Ni site. This coupling, which was shown to be of antiferromagnetic nature, leads to the formation of a bound state, the so-called

*robert.karsthof@physik.uni-leipzig.de

Zhang-Rice (ZR) bound state, with total spin $S = \frac{1}{2}$ in the case of NiO and thus being a doublet. This new view made it possible to explain as yet inexplicable features in photoelectron spectroscopy experiments, where the ZR doublet appears as the state with the lowest ionization energy. Taguchi *et al.* [18] also predicted an important role of this state in the electrical conduction process in NiO. However, to our knowledge, no attempt has been made so far to develop a conduction model taking the properties of ZR states explicitly into account. The high binding energies of the holes occupying these states imply that carrier transport takes place exclusively through these energetically rather isolated states without the participation of any other states or bands. Thus, the compatibility of the ZR with the interacceptor hopping model is given, and the validation of this attempt is the aim of the current work.

Recently, NiO has reemerged as a material of special interest in the device community. Its large band gap of around 4 eV [19,20] makes it transparent in the visible spectral range, and it is one of the rare examples of *p*-type semiconducting oxides. As such, it has found application in organic solar cells [21–23], light-emitting diodes [24,25], resistive-switching devices [26,27], perovskite solar cells [28], and electrochromic devices [29–32]. In many applications, efficient hole transport through the NiO layer is essential while, at the same time, the layer itself should be transparent in the visible and near-infrared spectral range. It is well known that the conductivity of NiO can be increased by intrinsic doping with Ni vacancies (through high oxygen supply during film growth) or by extrinsic doping, e.g., with group-I elements such as Li [23,33]. However, as the doping level is increased, the optical transmittance of NiO typically shows a marked decrease [19], which has recently been attributed to the development of a broad ZR band deep inside the band gap [34]. This behavior requires a trade-off between high optical transparency and electrical conductivity. The latter is typically not higher than 0.1 S cm^{-1} due to low hole mobilities ($\mu_p \leqslant 0.1$ cm^2 V^{-1} s^{-1}) of the localized charge carriers. In order to design NiO layers addressing the requirements for simultaneous conductivity and transparency, an understanding of the microscopic nature of carrier transport processes is necessary.

II. EXPERIMENTAL METHODS

The NiO films were prepared by two different methods. Pulsed laser deposition (PLD) growth was carried out in an in-house-built system, using a KrF excimer laser (wavelength 248 nm, pulse energy 650 mJ) ablating a ceramic NiO target (purity 99.998%; Alfa Aesar). PLD growth was done either at room temperature (no intentional substrate heating) or at a substrate temperature of 300 °C. In both cases, the partial pressure of the oxygen background atmosphere was set to 0.1 mbar. Reactive dc magnetron sputtering from a metallic Ni target in an Ar/O_2 atmosphere was additionally employed to grow NiO films. Layer thicknesses between 100 nm and 350 nm have been achieved and checked by means of profilometry; *c*-plane-oriented, one-sided polished Al_2O_3 single crystals were used as substrates. Metallic back contact layers consisting of Pt (thickness $\approx$ 50 nm) were deposited by dc magnetron sputtering in Ar atmosphere prior to NiO growth. The NiO layers were directly capped by a 20 nm thick Pt layer. NiO films and the respective Pt capping layers were deposited on top of a layer of photoresist patterned by UV photolithography. Liftoff of the photoresist was then used to produce pillar-shaped NiO/Pt contacts (diameters between 250 μm and 800 μm).

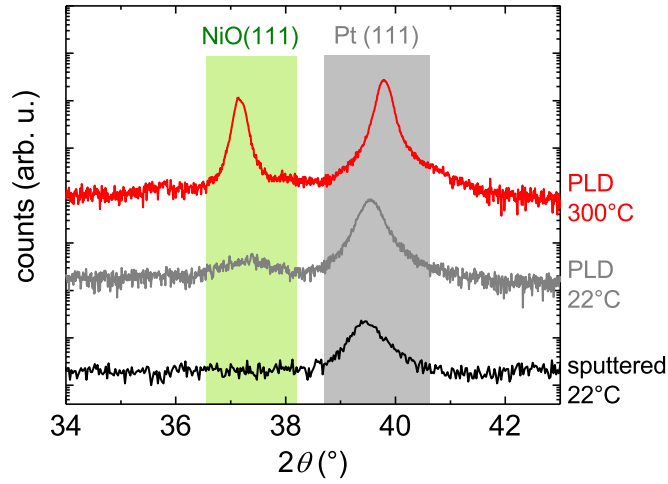

FIG. 1. X-ray diffraction pattern of the (111) reflexes of NiO grown on Pt/fused silica for PLD-grown and sputtered thin films at room temperature, as well as PLD-grown at elevated temperature.

Current-voltage characterization of the Pt/NiO/Pt structures was carried out with the help of a Süss wafer prober with tungsten needles and an Agilent 4155C precision semiconductor parameter analyzer. On the basis of these measurements, individual contacts were selected for further characterization. Those samples were then mounted onto transistor sockets, and the selected pillars were contacted by Au wire bonding using silver epoxy resin. Temperature-dependent current-voltage measurements on thusly prepared samples were done in a closed-cycle He cryostat.

Broadband dielectric spectroscopy (BDS) measurements have been accomplished on the same samples as used for current-voltage studies. The spectra have been recorded in a temperature and frequency range of 120 K to 300 K and 10^{-2} Hz to 10^{-7} Hz, respectively, employing a Novocontrol Technologies high-resolution α analyzer combined with a Quatro temperature controller ensuring absolute thermal stability of $\leqslant$ 1 K.

III. RESULTS

A. Structural properties

In the past, NiO has been deposited at room temperature in our laboratories using both methods, either PLD or sputtering, in order to fabricate active electronic devices [35–37]. However, these films exhibit high structural disorder, as evident from 2θ-ω x-ray diffraction scans shown in Fig. 1. While room-temperature PLD on top of a Pt back contact leads to nanocrystalline films where the (111) reflex of NiO can be observed, this peak is absent for the sputtered films. Using the Scherrer formula

$$l_z \approx \frac{0.9\lambda}{\Delta(2\theta)\cos(\theta)} \quad (1)$$

TABLE I. Parameters of NiO films fabricated by different methods, namely reactive dc magnetron sputtering ("ms-NiO") and PLD at room temperature and at 300 °C (RT-PLD- and HT-PLD-NiO, respectively): grain size l_z, net doping density N_{net} from *CV* measurements, and dc conductivity σ_{dc} at room temperature.

Sample	l_z (nm)	N_{net} (cm^{-3})	σ_{dc} (S cm^{-1})
ms-NiO	<5	1×10^{19}	9×10^{-4}
RT-PLD-NiO	≈ 30	4×10^{18}	3×10^{-6}
HT-PLD-NiO	$\geqslant 150$	1×10^{18}	3×10^{-8}

with $\lambda = 5.406$ Å (Cu Kα radiation), $\Delta(2\theta)$ FWHM of the reflex at position 2θ, the lower limit of the vertical expanse of the crystallites, l_z, can be estimated. On the one hand, for room-temperature PLD-grown NiO, l_z amounts to approximately 30 nm. On the other hand, the absence of the reflex for the sputtered films implies grains smaller than about 5 nm. In order to discriminate between effects arising from the crystalline structure and from the true bulk transport properties of NiO, PLD growth at an elevated temperature of 300 °C was studied as well. Such films grow in a highly (111)-oriented fashion, with a grain size, according to Eq. (1), of around 150 nm being of the same order as the film thickness of this sample.

B. Doping concentrations

Intrinsic doping of NiO is achieved by supplying excess oxygen during film growth. This leads to a high density of nickel vacancies (V_{Ni}), which is the dominant intrinsic point defect under oxygen-rich ambient conditions [33]. In the experiments reported here, this is achieved using both deposition methods by choosing a high oxygen background pressure ($p_{O2} = 0.1$ mbar and 0.018 mbar for PLD and sputtering, respectively). In order to determine the resulting carrier density for the particular growth conditions, films were grown on top of highly fluorine-doped tin oxide (FTO) layers (FTO-coated glass substrates were supplied by Calyxo GmbH, Germany; $\sigma_{FTO} = 2.5 \times 10^3$ S cm^{-1}), which induces a significant depletion region in the NiO layers. On these structures, capacitance-voltage (*CV*) measurements were conducted to determine the net doping density N_{net} of the films; Hall effect measurements can usually not be employed with NiO because of the absence of free carriers. Because *CV* is an ac technique and holes in NiO are expected to have a low mobility, it is important to choose the measurement frequency low enough that the charge carriers can follow the ac signal. Selected frequencies typically were between 100 Hz and 1 kHz depending on the noise level of the measurement. It was also ensured by frequency sweeps that the capacitance at the chosen frequency is at a plateau or at least only slowly changing with f, which is an indication that the error induced by unrecorded, slower contributions is negligible. The values for N_{net} obtained by *CV* measurements are given in Table I. In the further course of this report, N_{net} is interpreted as being equal to the carrier density. Table I demonstrates that reactive dc magnetron sputtering produces films with the highest net doping ($N_{net} \approx 10^{19}$ cm^{-3}), whereas high-temperature PLD-grown films have the lowest doping density (10^{18} cm^{-3}).

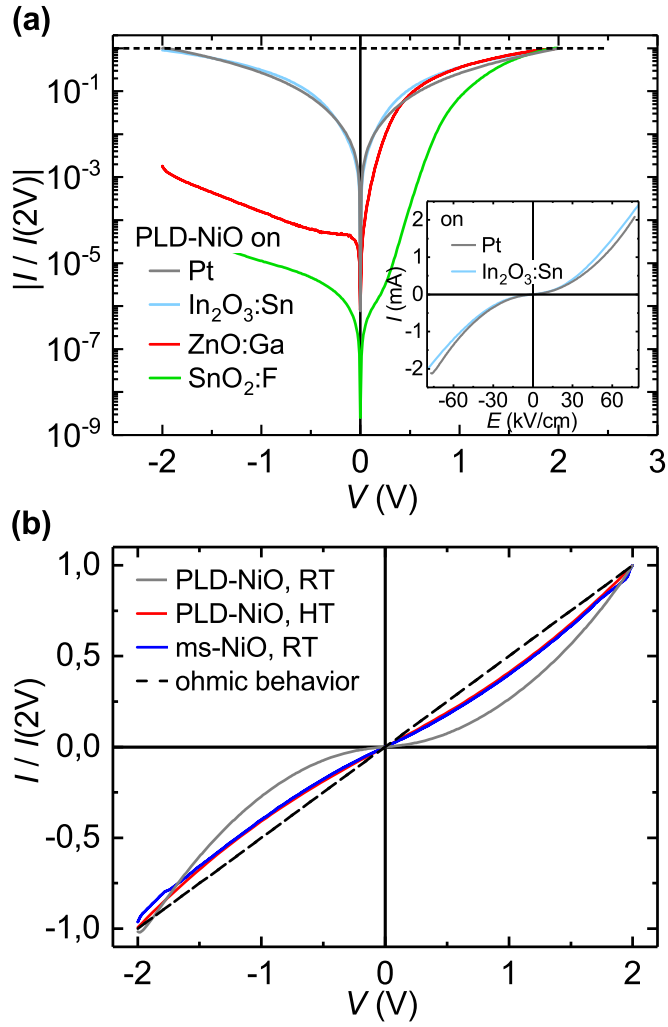

FIG. 2. (a) Typical current-voltage characteristics of room-temperature PLD-grown NiO on top of different conductive materials; absolute currents in log scale, normalized to currents at $V = 2$ V, for all back contacts. Inset: Currents for NiO on Pt and ITO as function of the applied dc electric field due to different NiO thicknesses (on ITO: 100 nm, on Pt: 260 nm). (b) Normalized currents for differently grown NiO layers, and ohmic characteristic for comparison.

C. Current-voltage characterization

The starting point for the investigations in this section is the general observation of non-ohmic dc transport in NiO thin films, even in the absence of a depletion layer. Figure 2(a) shows typical current-voltage relationships for NiO layers sandwiched between different conductive materials. Specifically, fluorine-doped tin oxide (FTO), tin-doped indium oxide (ITO), gallium-doped zinc oxide (GZO) (the latter two grown in-house by PLD), and Pt were used as bottom contacts, respectively. All samples were capped with a Pt top electrode. It can be seen that FTO and GZO back electrodes induce a depletion layer located almost exclusively within the NiO (hole density $p = N_{net} = 4 \times 10^{18}$ cm^{-3}), due to the high electron densities ($n > 5 \times 10^{19}$ cm^{-3}, determined by Hall effect measurements) in GZO and FTO layers. This depletion layer causes a significant current rectification. In the case of

ITO contacts, the rectification is hardly visible, and for the Pt back electrode the current-voltage characteristics are almost symmetric, indicating the absence of a depletion region. This can be understood based on the Anderson (or electron affinity) rule that uses the difference of Fermi energies of two materials in order to assess whether or not a depletion region forms between them. The Fermi energy of NiO typically lies about 5 eV below the vacuum level, slightly lower than for ITO (work function between 4.6 eV and 4.8 eV [38]) such that electrons enter the NiO and evoke hole depletion, but higher than for Pt (about 5.3 eV [39]), so no depletion layer is expected to form in this case.

Also in the absence of depletion, however, a clear deviation from a linear current-voltage relationship is present, as shown in the inset of Fig. 2(a). It can be seen that the *IV* characteristics (apart from a weak asymmetry in the case of ITO due to slight depletion) show very similar behavior, with a conductivity that increases with applied electric field. The similarity of the characteristics with respect to the two different contact materials, and the independence of the NiO thickness, implies that the observed behavior is intrinsic to the NiO layers and not an effect of a voltage-dependent carrier injection at the contacts.

Figure 2(b) displays normalized current-voltage characteristics for NiO layers grown by the different methods used in this work. The deviation from ohmic behavior (indicated by the dashed black line) can be seen for all samples, but is most pronounced for room-temperature PLD-grown layers. For this reason, these samples were chosen for further investigations of transport properties. It should be noted that although the characteristics match well qualitatively, the current densities are different for these three samples due to widely varying conductivities. Values for σ_{dc}, obtained by numerical differentiation of the current-voltage characteristics at a dc voltage of 0 V, are provided in Table I. It can be stated that there seems to be a strong nonlinear dependence of σ_{dc} on N_{net}, indicating that the role of the V_{Ni} acceptors probably goes beyond contributing extra charge carriers to the electronic system.

Nonlinear current transport in NiO has been reported before, e.g., on Pt/NiO/Pt [26] and ITO/NiO structures [40]. This behavior has been interpreted by Chang *et al.* in the framework of the space-charge-limited current (SCLC) model [41], which explicitly takes into account long transient times for charge carriers traveling through a low-mobility insulator after injection by ohmic contacts. These authors found an approximate $I \propto V^2$ relationship, indicating that the transport within the NiO layer is limited by hole trapping into electronic states with a single activation energy.

In Fig. 3, the temperature dependence of the *jV* characteristics of Pt/(RT)PLD-NiO/Pt structures is shown. Three different regions of the curves can be distinguished on a double-logarithmic scale: (i) ohmic conduction below 0.2 V $j \propto V$, (ii) a transition region where the slope of the curves increases, and (iii) a power-law region $j \propto V^{\gamma}$ with a temperature-dependent voltage exponent γ taking on values close to 2. It should be noted that in the data presented here, a slight exponential contribution to the current densities for temperatures above 260 K is detected in the voltage regime (iii) owing to a weak hole barrier located beneath the metallic Pt capping

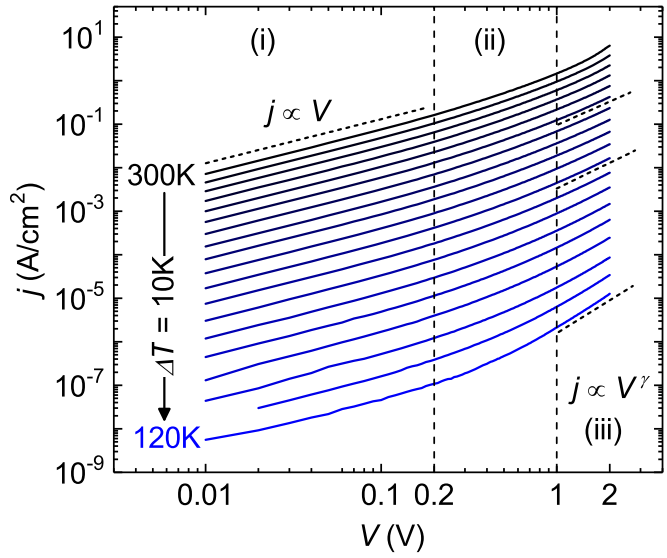

FIG. 3. Current density–voltage characteristics for one contact in double-logarithmic scale for temperatures between 300 K and 120 K.

layer. This behavior is observed when the capping layer is not deposited on top of the NiO immediately after semiconductor growth. We therefore think that it can be attributed to an out-diffusion of the mobile Ni vacancies in the vicinity of the NiO surface, thereby producing a downward bending of the bands that is conserved also after Pt deposition. We have tested this hypothesis by using different combinations of the noble metals Au, Pd, and Pt for both back and front contacts and found that the occurrence of a slight rectification is only dependent on the time between NiO and capping layer deposition, with the depletion layer always located below the top electrode. For temperatures $\leqslant 260$ K, however, the current densities are symmetrical with respect to the applied voltage, and therefore are probably determined solely by transport in the neutral NiO bulk material.

The temperature dependence of the voltage exponent γ is shown in Fig. 4. It is evident that below 220 K γ is linearly dependent on T^{-1}, increasing from a value of 1.92 at 220 K to 2.72 at 120 K. This behavior can be consistently explained in the framework of SCLC, taking into account trap states distributed over a certain energy range as proposed by Rose [41]. It can be shown that in this case, the relation

$$j \propto V^{1+\frac{T_c}{T}} \tag{2}$$

holds, with T_c a critical temperature characteristic for the broadness of the trap distribution. Fitting the data $\gamma(T^{-1})$ with a linear model yields $\gamma = 0.92 + \frac{216\ \mathrm{K}}{T}$, which is in agreement with Eq. (2). It can be concluded that the transport in NiO can be characterized as being due to holes trapped in a distribution of states. Rose [41] provided a method that allows us to determine the trap distribution on the basis of *jV* characteristics under the condition that $\gamma \geqslant 2$:

$$D_t = \frac{1}{dA}\frac{CV}{ek_BT}\left(\frac{V}{j}\frac{dj}{dV} - 1\right)^{-1} \tag{3}$$

with d and A being the thickness and area of the contact, respectively, and C its capacitance (85 pF, as determined from

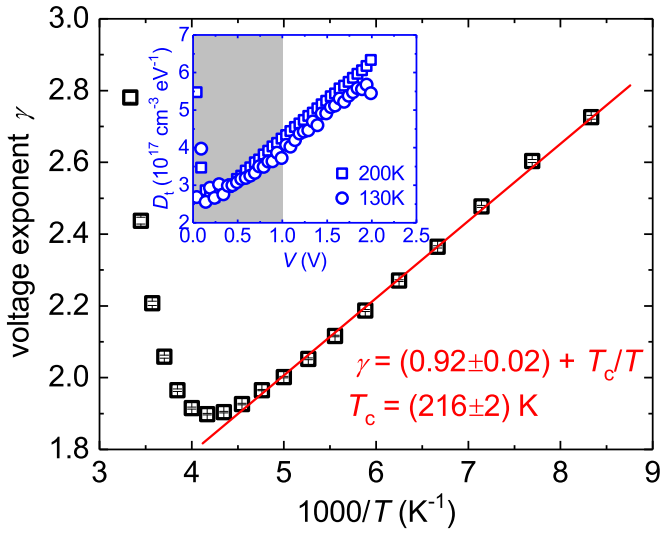

FIG. 4. Temperature dependence of the voltage exponent γ, and linear fit according to Eq. (2). Inset: Trap distribution calculated for $T = 200$ K and 130 K according to Eq. (3); gray area: ohmic and transition region where unphysical results are likely obtained.

quasistatic capacitance-voltage measurements). Equation (3) gives the number density of traps per unit energy interval. This calculation has been performed for two different temperatures, namely 200 K and 130 K; the results are shown in the inset of Fig. 4. It can be seen that the density of traps determining the admitted current density increases linearly with applied voltage. It is also worth noticing that the value of the probed density of states does not seem to depend on temperature in this range. The observed decrease of the electric conductivity can therefore be entirely ascribed to a drop of the charge carrier mobility.

Because the hole in NiO occupies a Zhang-Rice bound state, implications for the electric current transported by these states should be considered [18]. Due to the similarity of the current-voltage characteristics of differently deposited NiO layers in our labs, and also the ones reported in the literature, we are convinced that the non-ohmic behavior is specific to the intrinsic transport of ZR states. The following scenario is suggested as a possible explanation: The formation of the ZR states depends the presence of spins localized on Ni 3d states on the one hand, and of holes (e.g, in the O 2p band, around V_{Ni} sites, etc.) on the other hand. Because the application of an external voltage injects additional holes, their density is enhanced, thereby leading to a more pronounced ZR band. Since the number of injected carriers scales linearly with the applied voltage, a linear correlation between V and the ZR density of states can be expected, which is exactly what is observed (inset of Fig. 4). This process might be of importance for the resistive switching behavior of NiO thin films, in which the conductivity changes abruptly upon applying a critical set voltage. This has already been attributed to the injection-induced formation of conductive filaments [42,43]. It should be noted that this effect was never observed on NiO films investigated in this work because of their comparatively high conductivities. Resistive switching is usually observed in films that exhibit insulating behavior in their pristine state.

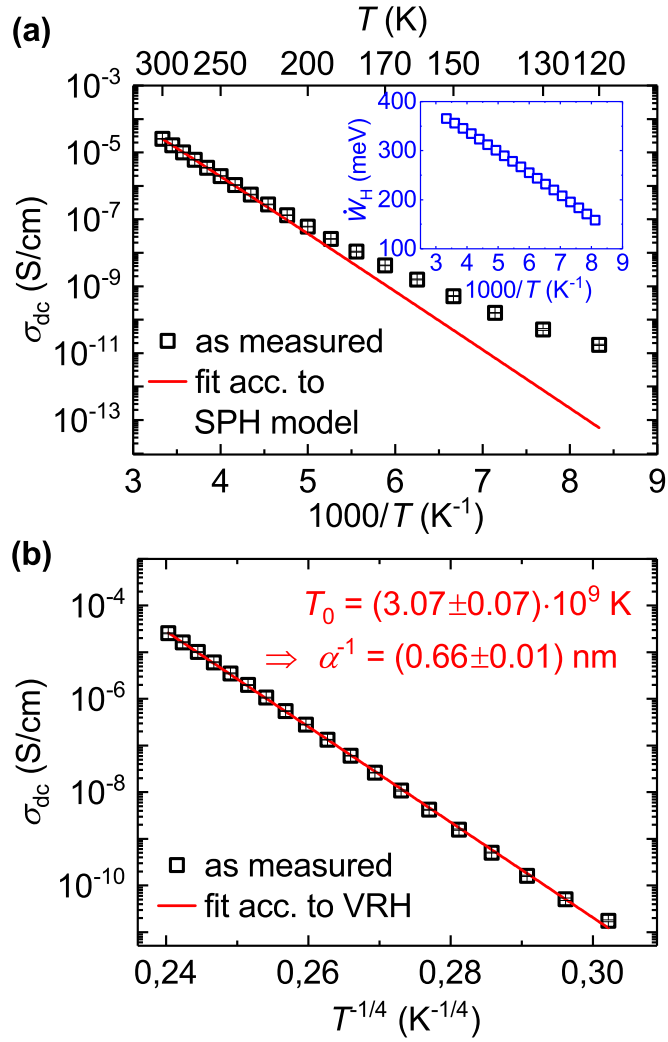

FIG. 5. Temperature dependence of the dc conductivity of PLD-grown NiO, obtained by numerical differentiation of the data from Fig. 3, and fits according to (a) the small polaron hopping model and (b) Mott variable range hopping. Inset in (a) shows the temperature dependence of the apparent hopping energy.

Figure 5(a) shows the temperature dependence of the conductivity as extracted from the data shown in Fig. 3 by numerical differentiation, for $V_{dc} = 0$ V. As can be seen, the conductivity decreases when the temperature is lowered. Furthermore, the thermal activation deviates from a single Arrhenius type as is evident from a kink of the curve at around 200 K. To describe the T dependence of the conductivity σ_{dc} of NiO, a transport model based on the hopping of "free" small polarons has been used in recently published works [34,44]. Within this model, the simplified expression

$$\sigma_{dc} = \sigma_0 \exp\left(-\frac{W_H}{k_B T}\right)$$

$$\text{with} \quad \sigma_0 = \frac{N e a_0^2 \nu_{ph}}{k_B T} \tag{4}$$

holds [6,45] with the polaron hopping activation energy W_H, carrier density N, a_0 lattice constant, and ν_{ph} optical phonon frequency. In Fig. 5(a), fits according to Eq. (4) are shown.

It is obvious that this model can reproduce the data only for temperatures above approximately 200 K. For lower temperatures, the small polaron hopping (SPH) model predicts considerably smaller values of σ_{dc} than experimentally determined, owing to a decrease of the activation energy with falling temperature. This is exemplified in the inset of Fig. 5(a), where the apparent SPH activation energy, $\dot{W}_H = \frac{\partial \ln(\sigma_{dc}T)}{\partial T^{-1}}$, is plotted. A drop in W_H is included in more elaborate models of small polaron hopping [46]. Therein, the drop evolves at temperatures of about one half of the Debye temperature $\frac{\theta_D}{2}$, which is indeed approximately 200 K for NiO [47]. Apart from that, however, a renewed *increase* of the conductivity σ_{dc} is to be expected at further decreasing temperatures due to the onset of polaronic band conduction. This has not been observed in the NiO samples investigated in this work down to temperatures of 20 K. Moreover, the extracted carrier mobilities are extremely low—at room temperature, $\mu = \frac{\sigma_{dc}}{eN_{net}} \approx 10^{-6}\,cm^2\,V^{-1}\,s^{-1}$, assuming the carrier density from CV measurements, $N_{net} = 4 \times 10^{18}\ cm^{-3}$. We suggest discarding hopping conduction of "free" small polarons as a current transport mechanism in doped NiO. The fact that the carriers are of polaronic character, however, is not questioned here, because this is an inherent feature of the bound ZR state [16]. We propose to interpret the data in the framework of the polaronic impurity hopping conduction as described by Schnakenberg [48]. Within this model, the carriers are small polarons transported by hopping, but they cannot move to any lattice site. Instead, their propagation is limited to defect sites to which they are tightly bound—a situation readily applicable to carriers occupying ZR bound states. In this model, the conductivity follows the same temperature dependence as in the "free" small polaron hopping, exhibiting a significant drop of activation energy at about $\frac{\theta_D}{2}$. The model differs only at low temperatures, where σ_{dc} continues to decrease according to $\exp(-\frac{A}{k_B T})$, where A is an activation energy on the order of the mean energy separation $\Delta\epsilon$ between neighboring defect sites. Band conduction is suppressed in this case due to the strong localization and large intersite separation. This model has already been applied to Li-doped NiO [15,49], and it is applicable to intrinsically (V_{Ni}-)doped NiO. In this case, however, the term "polaronic interacceptor hopping" is more appropriate because V_{Ni} defects are not impurities in a chemical sense.

Carrier hopping between defect states randomly distributed in space and energy (in a sufficiently large range $\Delta\epsilon$) can also be described within the model of variable range hopping (VRH) developed by Mott [50]. There, the relation

$$\sigma_{dc} = \sigma_0 \exp\left(-\left[\frac{T_0}{T}\right]^{\frac{1}{4}}\right) \tag{5}$$

holds, with a characteristic temperature

$$T_0 \approx \frac{20\alpha^3}{k_B N(\epsilon_F)}, \tag{6}$$

which is determined by the localization length α^{-1} of the carriers and the density of states at the Fermi energy $N(\epsilon_F)$. In Fig. 5(b), the measured dc conductivity is plotted logarithmically against $T^{-\frac{1}{4}}$ together with a fitting curve according to Eq. (5), and it can be seen that the VRH model reproduces the data over the entire temperature range investigated here. The characteristic temperature amounts to $(3.07 \pm 0.07) \times 10^9$ K. If one takes the acceptor density of states $N(\epsilon_F) = D_t = 2.6 \times 10^{17}\ cm^{-3}\ eV^{-1}$, as obtained from the jV characteristics by extrapolating the density of states in Fig. 4 to $V = 0$ V, the localization length of a polaron in a ZR state amounts to $\alpha^{-1} = (0.66 \pm 0.01)\,nm \approx 1.6 a_0$.

One might object to using the VRH model in the entire temperature range because this model has originally been developed for transport at low temperatures only. However, Böttger and Bryksin [46] formulate a criterion that can be employed for justifying the use of this model also at higher temperatures. When the energetic distribution of the acceptor states $\Delta\epsilon$ is narrow, such that

$$\alpha N_{net}^{-\frac{1}{3}} \gg \frac{\Delta\epsilon}{k_B T} \tag{7}$$

holds true, next-neighbor hopping occurs. When Eq. (7) is not fulfilled, VRH is favored. In the present case, $N_{net} = 4 \times 10^{18}\ cm^{-3}$, $\alpha = 1.5 \times 10^9\ m^{-1}$, and $\Delta\epsilon \approx 200$ meV (as extracted from the apparent activation energy of σ_{dc} at low temperatures), such that at room temperature $\alpha N_{net} = 9.4 \gg \frac{\Delta\epsilon}{k_B T} \approx 8$. Thus, the VRH model can be applied at least up to room temperature. It can be comprehended as a limiting case of the interacceptor hopping model for large energy spread $\Delta\epsilon$ of the defect states. Such a broad energetic distribution can be expected due to the high degree of disorder in the RT-deposited NiO films leading to the formation of other defects or defect complexes, some of which are donor-like. This causes a large degree of compensation. In fact, for the occurrence of charge transport, partial compensation is always necessary, because otherwise all acceptors are charge-neutral, and no free target states are available for hopping.

D. BDS measurements

In this section, the temperature-dependent behavior of the complex conductivity $\sigma^* = \sigma' + \imath\sigma''$ of NiO thin films is discussed, comparing the sample grown by PLD at room temperature ("RT-PLD") and the one at 300 °C ("HT-PLD"). Figures 6(a) and 6(b) show the real part of the conductivity, σ', measured by broadband dielectric spectroscopy (BDS) between room temperature and 120 K and in a frequency range from 10^{-2} Hz to 10^7 Hz (RT-PLD) or 3×10^6 Hz (HT-PLD). In the latter case, the data obtained above 3×10^6 Hz were discarded due to the occurrence of inductance-induced artifacts. Measurements were taken while cooling to 120 K as well as during heating back to room temperature in order to check for the reproducibility. Measurements were done at a dc voltage of 0 V; the amplitude of the ac voltage was set to 10 mV such that the response of the sample is measured in the ohmic voltage region.

Two different features dominate the behavior of σ': (i) a frequency-independent contribution at low frequencies appearing as a plateau and interpreted as the dc conductivity limit σ_{dc}, as well as (ii) a dispersive part where σ' increases with frequency. In the case of the RT-deposited film, σ_{dc} gradually decreases over more than 6 orders of magnitude

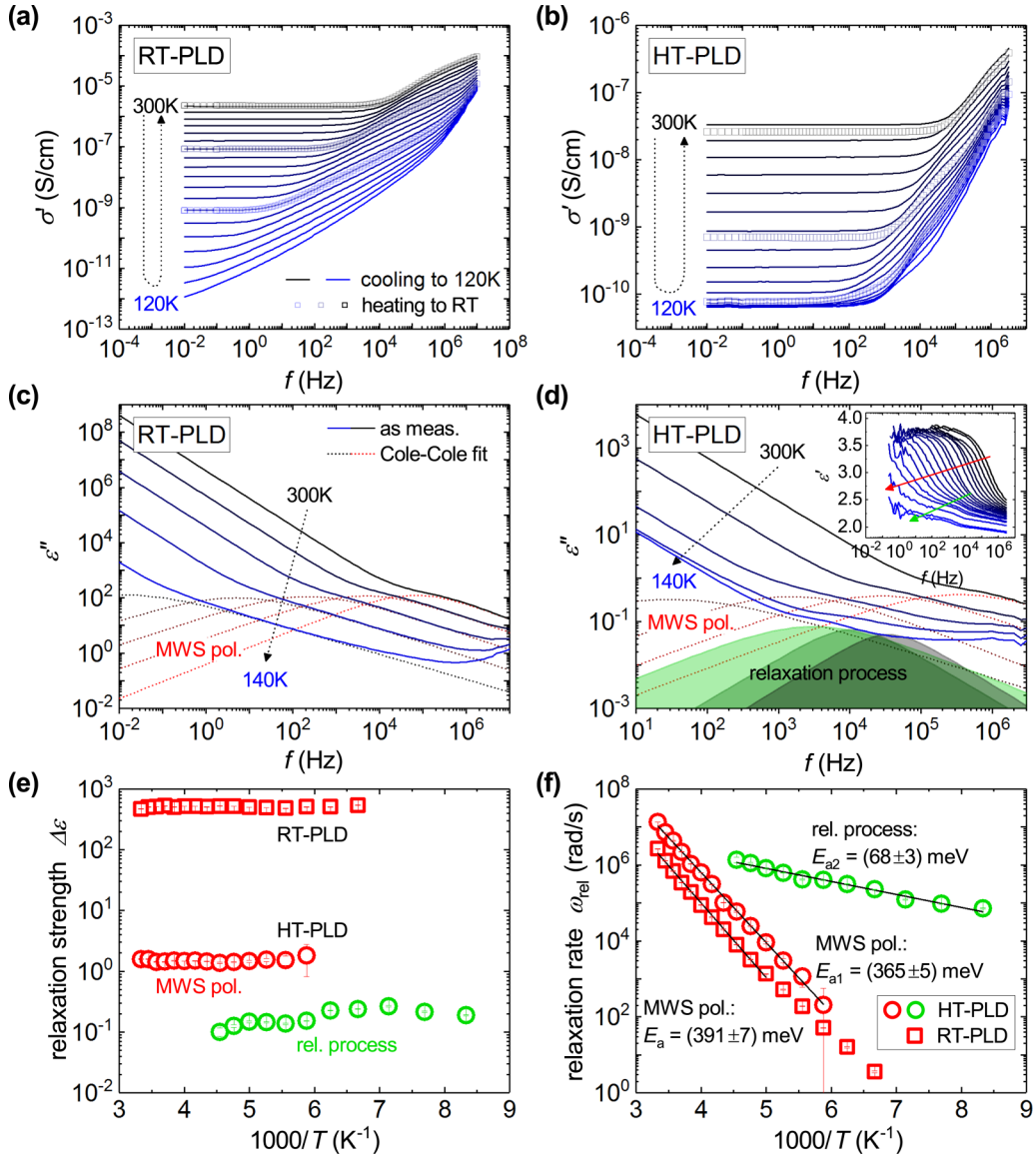

FIG. 6. Frequency and temperature dependence of (a), (b) the real part σ' of the complex conductivity $\sigma^* = \sigma' + \imath\sigma''$, and (c), (d) the imaginary part ε'' of the complex dielectric function $\varepsilon^* = \varepsilon' - \imath\varepsilon''$, for (a), (c) the room-temperature- and (b), (d) high-temperature-deposited NiO film for selected temperatures, together with fits of the relaxation processes according to Eq. (9). Inset in (d): Real part of dielectric function for all temperatures, arrows indicating steps due to the two relaxation processes. (e) Relaxation strengths $\Delta\varepsilon$ and (f) relaxation rates $\omega_{\text{rel}} = \frac{2\pi}{\tau_{\text{rel}}}$ of the identified processes.

within the investigated temperature range, whereas for the HT-NiO it drops by approximately 3 orders of magnitude down to approximately 200 K and remains almost constant below that temperature.

The complex dielectric function ε^* can be calculated from the complex conductivity σ^* via the relation

$$\varepsilon^* = \frac{1}{\imath\omega\varepsilon_0}\sigma^*. \tag{8}$$

In Figs. 6(c) and 6(d), the imaginary part of ε^*, $\varepsilon'' = \frac{1}{\omega\varepsilon_0}\sigma'$, is plotted. It becomes evident that the dispersion of σ' is due to the occurrence of dielectric relaxation phenomena, expressed as peaks or shoulders on the high-frequency side of the dc conductivity term ($\propto \omega^{-1}$). These relaxation processes can be described with the Cole-Cole equation [51]

$$\begin{aligned}
\varepsilon^*_{\text{CC}}(\omega) &= \varepsilon'_{\text{CC}}(\omega) + \imath\varepsilon''_{\text{CC}}(\omega) \\
&= \varepsilon_\infty + \frac{\varepsilon_s - \varepsilon_\infty}{1 + (\imath\omega\tau_{\text{rel}})^{1-b}}, \\
\varepsilon'_{\text{CC}} &= \varepsilon_\infty + \frac{\varepsilon_s - \varepsilon_\infty}{2} \\
&\quad \times \left[1 - \frac{\sinh\left[(1-b)\ln(\omega\tau_{\text{rel}})\right]}{\cosh\left[(1-b)\ln(\omega\tau_{\text{rel}})\right] + \cos b\pi/2}\right], \\
\varepsilon''_{\text{CC}} &= \frac{\varepsilon_s - \varepsilon_\infty}{2} \frac{\cos b\pi/2}{\cosh\left[(1-b)\ln(\omega\tau_{\text{rel}})\right] + \sin b\pi/2},
\end{aligned} \tag{9}$$

which is a Debye-type function with symmetric broadening. The parameters $\Delta\varepsilon = \varepsilon_s - \varepsilon_\infty$, $b \in [0, 1)$, and τ_{rel} represent

the relaxation strength, relaxation process broadening, and relaxation time, respectively. Based on Eq. (9), and by adding the dc conductivity term ($\varepsilon'' = \varepsilon''_{CC} + \frac{\sigma_{dc}}{\omega\varepsilon_0}$), the ε'' data have been fitted to extract the respective relaxation process parameters and the dc conductivity. These fits are included in Figs. 6(c) and 6(d) as color-shaded areas. The fit parameters $\Delta\varepsilon$ and $\omega_{rel} = \frac{2\pi}{\tau_{rel}}$ and their temperature dependence are shown in Figs. 6(e) and 6(f). The data for the broadening parameter b are not presented.

In the case of the RT-grown film with high structural disorder, only one relaxation process is visible. It possesses a generally high relaxation strength $\Delta\varepsilon \approx 500$ that is almost independent of temperature [Fig. 6(e)]. The film with low disorder exhibits two relaxation processes, the stronger of which appears between room temperature and about 170 K, while the weaker process is only visible below 230 K. For reasons explained in the following, the relaxation process in the RT-deposited sample and the stronger one in the HT-deposited film are probably due to the same mechanism; this process will be analyzed first.

For a process caused by relaxation of molecular dipoles of density N_{dip} and dipole moment μ_{dip}, $\Delta\varepsilon$ at a certain temperature can be estimated by the relation

$$\Delta\varepsilon \approx \frac{1}{\varepsilon_0}\frac{\mu_{dip}^2}{k_B T} N_{dip}. \tag{10}$$

If one assumes that the dipoles consist of two charges $\pm e$ at a distance of one NiO lattice spacing a_0, and the dipole density is given by the trapped-hole density, $N_{dip} \approx 1 \times 10^{18}$ cm^{-3}, the corresponding relaxation strength at room temperature, according to Eq. (10), would be on the order of 0.1, which is three orders of magnitude lower than the $\Delta\varepsilon$ observed in the RT-deposited film and a factor of 10 lower than in the HT-NiO sample. In addition, Eq. (10) implies a decrease of $\Delta\varepsilon$ with increasing temperature; however, such a decrease is absent in the measurements. Therefore, a molecular relaxation mechanism can be excluded as assignment for this relaxation process. Instead, an explanation is provided on the basis of the crystalline structure of the investigated films, which causes a spatial inhomogeneity of the electrical conductivity. Such mesoscopic inhomogeneities are known to cause interfacial polarization effects, subsumed under the term *Maxwell-Wagner-Sillars (MWS) polarization* [52]. Models of this type of effect typically consider particles with a high electrical conductivity embedded in a matrix of lower conductivity, which can be identified with conductive NiO grains separated by insulating grain boundaries. Consequently, an ac electric field induces a spatial separation of charge carriers within the grains. A characteristic of an MWS process is an abnormally high and temperature-independent relaxation strength ($\Delta\varepsilon \gg 1$, determined by the conductivity contrast between the two components and the filling ratio of the particles). It must be said that for the inverted case, i.e., insulating particles surrounded by a conductive matrix, it can be shown that interfacial polarization appears as well, however, in association with a much lower apparent relaxation strength [53], $\Delta\varepsilon < 1$. This is not compatible with our data, which is why we argue in favor of NiO particles/grains that exhibit higher electrical conductivity in their interior than on their surface.

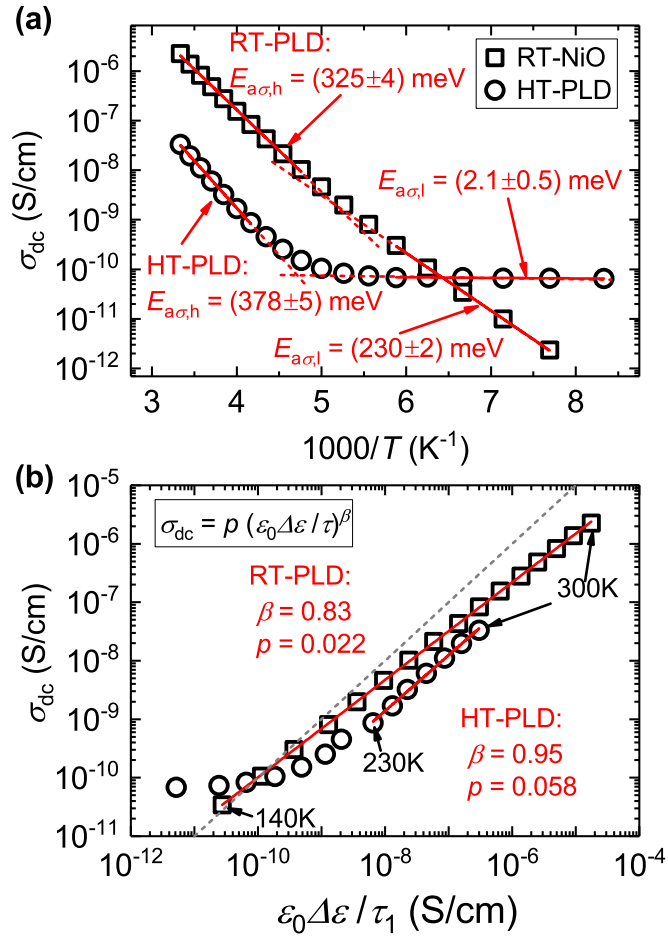

FIG. 7. (a) Temperature dependence of the dc conductivity for the RT- and HT-deposited sample as extracted from the frequency-dependent measurements, with Arrhenius fits and respective activation energies. (b) Barton-Nakajima-Namikawa (BNN) relation for the strong-relaxation process observed in both samples; gray line indicates the ideal ($p = 1$, $\beta = 1$) relationship.

Typical for disordered materials with a distinct dc conductivity plateau is a dielectric relaxation process visible at frequencies that are too high for the mechanism causing the dc conductivity (usually a molecular hopping process) [54]. The correlation between σ_{dc} and the relaxation strength and rate is described by the so-called *Barton-Nakajima-Namikawa (BNN) relation*:

$$\sigma_{dc} = p\,\varepsilon_0\Delta\varepsilon\,\omega_{rel}. \tag{11}$$

Here, p is a numerical constant on the order of unity, typically between 0.5 and 10, and independent of temperature. Because the T dependence of $\Delta\varepsilon$ is typically much weaker than that of σ_{dc}, Eq. (11) implies that $\sigma_{dc} \propto \omega_{rel}$. In addition, if the dc conductivity is temperature-activated with a particular activation energy, ω_{rel} should show the same dependence. This has been checked for the investigated NiO films and is shown in Figs. 7(a) and 7(b). In the temperature region between 300 K and about 240 K, where σ_{dc} shows a temperature-activated behavior, the activation energies are 325 meV and 378 eV for the RT and HT samples, respectively, which is close to the activation energies for the relaxation process in question

[(391 meV and 365 meV; see Fig. 6(f)]. In Fig. 7(b), it can be seen that the BNN relation between the dc conductivity and the relaxation parameters is fairly satisfied in the range where σ_{dc} is temperature-activated; for the HT-NiO sample, this excludes the low-temperature regime. The relationship between σ_{dc} and the "reduced relaxation strength" $\varepsilon_0 \Delta\varepsilon\, \omega_{rel}$ is, however, slightly sublinear, and the parameter p takes on values on the order of $10^{-2} \ll 1$. Such a low value of the BNN parameter p is far outside the range expected for a microscopic origin of the relaxation process. The similarity of the activation energies of σ_{dc} and ω_{rel} is, on the other hand, a typical signature of an MWS polarization process [52]. Within a simplified model that considers spherical filler particles (volume fraction φ_f) of conductivity σ_f' inside a matrix of conductivity σ_m' with $\sigma_m' \ll \sigma_f'$, filling fraction $\varphi_m = 1 - \varphi_f$, and an identical real part of the dielectric function ε' for both phases, it can be shown that a Debye-type relaxation occurs [52], with

$$\Delta\varepsilon \approx 3\varepsilon' \left(\frac{\sigma_f'}{\sigma_m'}\right)^2 \frac{\varphi_f(1-\varphi_f)}{(2+\varphi_f)^2},$$
$$\tau_{rel} \approx 3\varepsilon_0\varepsilon' \frac{1}{\sigma_f'(1-\varphi_f)}. \tag{12}$$

Equations (12) demonstrate that, on the one hand, the relaxation strength is determined by the squared ratio of the conductivities σ_f and σ_m. The temperature dependencies of both are similar and therefore roughly cancel out, and $\Delta\varepsilon$ becomes only weakly temperature-dependent. On the other hand, the relaxation rate $\omega_{rel} \propto \tau_{rel}^{-1}$ is directly proportional to σ_f, and therefore a BNN-relation-like correlation is obtained. Equations (12) are, however, only valid under rather strict conditions regarding the filling fraction φ_f and the shape of the filler particles, and are therefore only used for constructing the qualitative arguments and not for quantitative analysis here. In any case, it can be stated that the difference in relaxation strength of the intense process is caused by a lower degree of disorder in the HT-grown film as compared to the RT-grown one, causing a reduced spatial inhomogeneity of the conductivity.

One may ask whether this polarization process renders the previously mentioned *CV* measurements unreliable, because it causes a large share of the RT-grown sample's capacitance at and below audio frequencies around room temperature, where these measurements were recorded. The capacitance of the depleted films used for *CV* characterization is in the range of 500 pF, which is a factor of 6 larger than the value for the undepleted films (about 85 pF). The overestimation of the net doping density caused by the MWS process therefore amounts to 34% of its value, because $N_{net} \propto C^2$. The net doping of the RT-grown film is therefore approximately 2.6×10^{18} cm^{-3}.

Next, the weaker relaxation process observed in the low-disorder sample is considered, which is only visible below 230 K. Above this temperature, it is potentially masked by the more intense MWS process, although there seems to be an abrupt qualitative change [which can be well seen in ε'; see inset of Fig. 6(d)] exactly at 240 K [Fig. 6(d)]. This process has a much lower relaxation strength $\Delta\varepsilon \approx 0.1$ than the MWS process [see Fig. 6(e)], which also shows a slight decrease with increasing temperature. Both facts are in accordance with a microscopic hopping process. The relaxation rate of the process is activated with an energy of 68 ± 3 meV [Fig. 6(f)].

To interpret these observations, the Schnakenberg model for a conduction process due to polaronic defect hopping [48] is considered again. Within this framework, there are three regions to be expected for the behavior of σ_{dc} with temperature: At high temperatures, $\sigma_{dc} \propto \exp(-\frac{W_H}{k_B T})$, where W_H is the average energy barrier between two neighboring defect sites. Due to spatial overlap of the polaronic wave functions, W_H is dependent on the average distance between two sites, decreasing with rising defect density. Hopping is achieved by multiphonon absorption (acoustical and optical) in this range. As the temperature drops to around $\frac{\theta_D}{2}$, the number of available optical phonons is lowered such that the critical hop is determined by single optic phonon absorption; here, the conductivity is proportional to the number of available optic phonons, $\sigma_{dc} \propto \exp(-\frac{\hbar\omega_{opt}}{k_B T})$, with ω_{opt} a typical optical phonon frequency. As the temperature decreases further, only acoustic phonons are available; the activation energy for hopping in this range is on the order of the energy width $\Delta\epsilon$ of the acceptor distribution. This behavior is most clearly shown by the low-disorder sample: here, above approximately 250 K, σ_{dc} is activated with $E_{a\sigma,h} = 378$ meV, while at low temperature, the conductivity shows a very weak temperature dependence with $E_{a\sigma,l} \approx 2.1$ meV. These two regions are separated by a temperature of approximately 200 K, which is indeed about half the Debye temperature. This temperature was already identified as a critical one during the discussion of the dc electric properties above. A similar change in activation energy can be seen for the RT-grown NiO, although it is not as pronounced. This can be explained by the much broader distribution of acceptor states in this sample due to a higher degree of disorder. For the HT-grown NiO, the distribution of acceptor states is highly confined in energy. For this reason, the VRH model cannot be applied to this sample, as was done before for the RT-grown one, because for this model the defect states have to be randomly distributed both spatially and energetically.

In the temperature range around $\frac{\theta_D}{2}$, the conductivity should vary as $\exp(-\frac{\hbar\omega_{opt}}{k_B T})$. This is difficult to evaluate because the region between the high- and low-temperature activated terms is narrow. However, the occurrence of the second relaxation process in the low-disorder sample can be taken as an indication for single-phonon processes determining the critical hop because the activation energy of the relaxation process is close to the energies of the optical phonons at the Γ point of NiO: $\hbar\omega_{TO} \approx 49$ meV, $\hbar\omega_{LO} \approx 72$ meV [55]. Extrapolating the relaxation rates to $T^{-1} = 0$ gives an attack frequency of the hopping process of $\omega_\infty = (4.23 \pm 0.96) \times 10^7$ rad s. According to the standard small polaron theory [56], the temperature dependence of the maximum of dielectric loss due to hopping is

$$\omega_{rel} = \omega_\infty \exp\left(-\frac{E_a}{k_B T}\right)$$
$$= \omega_{opt} \exp(-2\alpha R) \exp\left(-\frac{E_a}{k_B T}\right), \tag{13}$$

where the first exponential term represents the magnitude of spatial overlap between two sites at a distance R. Using Eq. (13) and estimating $R = (\frac{3}{4\pi}N_{\text{net}}^{-1})^{\frac{1}{3}} = 6.2\,\text{nm}$ for the HT-grown NiO film, the localization length α^{-1} of the charge carriers localized at one V_{Ni} acceptor site can be estimated as $\alpha^{-1} \approx (0.85 \pm 0.01)\,\text{nm} \approx 2a_0$. This value is close to the one obtained from the dc measurements on RT-NiO in the first section of this paper, where 0.66 nm was obtained. The charge carriers in the RT-grown film seem to be more localized than in the low-disorder sample.

Lunkenheimer *et al.* have investigated the ac electrical conductivity of reactively e-beam-evaporated NiO thin films and have applied the model of correlated barrier hopping (CBH) to explain the observed frequency and temperature dependence of σ^* [12]. The authors also reported on a relaxation process visible at audio frequencies with a relaxation rate that is activated with an energy of around 300 meV. They interpreted this as a manifestation of the cutoff of the carrier hopping process. From the data given in the article, however, it can be estimated that the relaxation strength of the process is $\Delta\varepsilon \approx 5$, which is too large for a molecular process. One may therefore discuss whether Lunkenheimer *et al.* also measured the dielectric response of a system exhibiting a spatially inhomogeneous conductivity. In any case, it is interesting to note the physical similarity of the CBH model and the defect hopping model. Both consider the transfer of charge carriers between neighboring acceptor (or donor) sites by thermal activation over an energy barrier the height of which depends on intersite separation.

Two comments on the dc conductivities σ_{dc} measured by broadband dielectric spectroscopy (BDS) shall be made. The first one concerns the agreement between these results and those obtained from *IV* measurements in the first section. They agree very well in the temperature range between 300 K and 200 K. Below that temperature, however, σ_{dc} as extracted from BDS measurements decreases more strongly than in the data obtained from *IV* characteristics; at 120 K, the values differ by about one order of magnitude. This is due to the fact that *IV* characteristics are not measured under static conditions, because a voltage ramp is swept through. Therefore, frequency-dependent currents, like the MWS polarization process, can contribute to the current signal. If the $\log \sigma_{\text{dc}}$ values from BDS measurements are plotted versus $T^{-\frac{1}{4}}$, however, the T_0 value characterizing the VRH conduction, and thereby also the localization length α^{-1}, is very similar to the one obtained before [$T_0 = (3.63 \pm 0.04) \times 10^9\,\text{K}$ and $\alpha^{-1} = (0.63 \pm 0.02)\,\text{nm}$, respectively] such that the main assertions of the first section remain essentially untouched.

The second comment concerns the difference of σ_{dc} between the HT- and the RT-grown samples at low temperatures. One may wonder why the former one exhibits a higher conductivity in this range, although the density of acceptor states is lower by a factor of about four. A possible answer is provided by the width of the energetic distribution of the impurities, which is much smaller in the weakly compensated HT-grown film ($\Delta\epsilon_{\text{HT-PLD}} \approx 2$ meV vs $\Delta\epsilon_{\text{RT-NiO}} \approx 230$ meV). A better energetic alignment of the states can facilitate a direct transfer of carriers between neighboring impurities by tunneling. This change in transport character from hopping to tunneling is also reflected by the fact that the position of both dielectric relaxation processes is not coupled to the magnitude of σ_{dc} in the low-temperature regime: both processes continue to shift to lower frequencies until they are partially or even completely masked by the constant-conductivity term.

We want to note that there may be an alternative explanation for the higher σ_{dc} in the low-disorder sample at low T, which is based on a possible enhancement of the acceptor state density on the surfaces of the grains. The crystallite size in growth direction has been shown to be on the order of the film thickness. However, by using scanning-electron microscopy on ion-beam-prepared cross sections of the high-temperature-grown films, it could be shown that the crystallites (for both Pt and NiO) grow in a columnar fashion with lateral diameters of about 50 nm. This can be explained by the sixfold rotational symmetry of the used *c*-oriented corundum substrate which invokes two rotational domains of the (111)-oriented layers growing on top. It is not immediately evident that the surfaces of the coalescent NiO grains are electrically insulating. If they exhibited a density of acceptor states that is enhanced in comparison to the interior of the crystallite, these states could provide a conductive path due to the spatial overlap of the localized states' wave functions. This possibility can only be ruled out by performing experiments on layers with larger lateral crystallite dimensions. That can be achieved, i.e., by using cubic substrates on which the Pt and NiO films grow without rotational domains, like the (111)-plane of MgO. The main assertion of this paper, namely, that a conductive path in doped NiO is provided by spatially overlapping acceptor states, applies for this case as well. However, the interpretation of the low-temperature region with its low activation energy of about 2 meV would then imply activated hopping over a significantly reduced energetic barrier.

Although the existence of strong interfacial (MWS) polarization also in the case of HT-NiO is in accordance with insulating grain surfaces, as discussed further above, this applies only for those surfaces oriented perpendicular to the ac electric field. Those oriented parallel to it, i.e., the interfaces between coalesced columnar domains, cannot be polarized by the electric field and may therefore be more conductive than the grain interior.

E. Summary of the proposed transport model

The conduction model for intrinsically doped NiO constructed in this paper is summarized in Fig. 8. It is based on holes trapped on V_{Ni} sites due to the formation of (small-polaron-like) bound Zhang-Rice states, and their direct transfer between such sites [Fig. 8(a)]. Because of the strongly bound character of these quasiparticles, any extended valence band states are sufficiently far away in energy that they can be neglected in the conduction process. At high temperature ($T > \frac{\theta_{\text{D}}}{2}$), the charge carriers hop over the energetic barrier between defects by multiphonon absorption. The activation energy of this process is similar (around 350 meV) for high- and low-disorder NiO because it depends only on the intersite separation. When $T < \frac{\theta_{\text{D}}}{2}$, hopping over the barrier is suppressed; in this regime, the current is carried by phonon-assisted tunneling through the barrier. The activation energy for this process is given by the energetic broadening of the

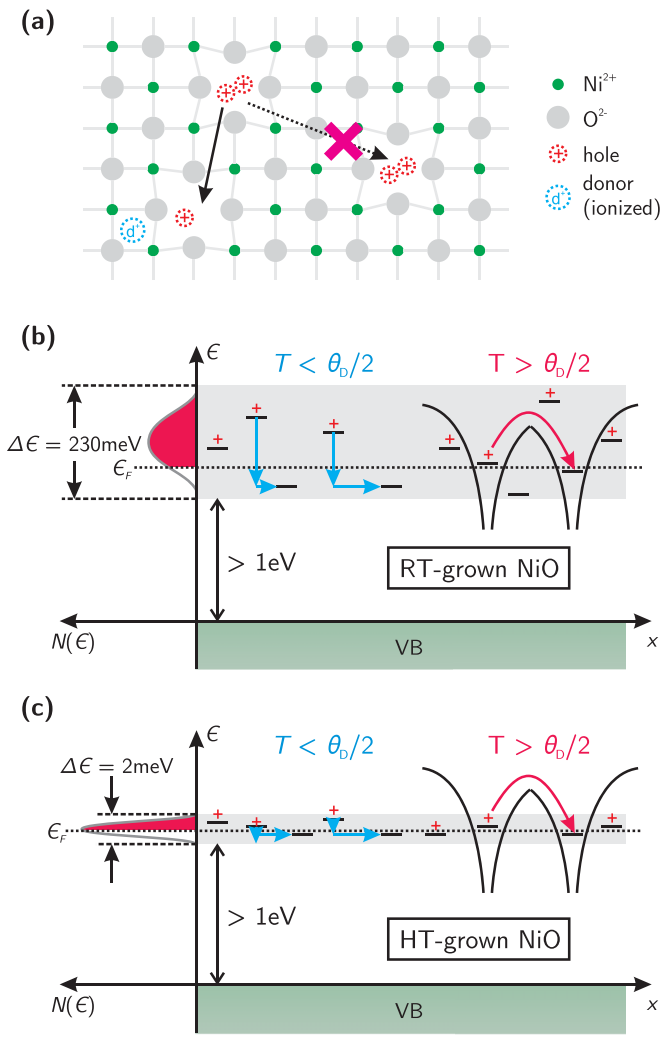

FIG. 8. Illustration of the proposed conduction model. (a) Transport is carried by holes propagating exclusively on Ni vacancy sites. Partial compensation by donors is necessary to enable charge transfer. (b) High degree of structural and electronic disorder introduces a broad distribution of deeply lying defect states in RT-grown NiO. For the low-disorder sample (c), the acceptor states are considerably more confined in energy. The temperature $T = \frac{\theta_D}{2} \approx 200\,\mathrm{K}$ separates two regimes with different hopping characteristics. Energies and spatial distances are not to scale.

defect-state distribution, which is lower for the low-disorder sample [Fig. 8(c)]. Because most states lie within a narrow interval around the Fermi energy, the current carried by this process is more efficient than in the high-disorder, room-temperature-grown sample, where fewer defect states with a similar energy level are available. Furthermore, for this sample, the states are widely distributed such that the VRH model applies at all temperatures below 300 K. In contrast to this, for the HT-NiO film, the narrow distribution of states allows charge transfer only between nearest-neighbor defects.

Based on this model, an explanation can be given as to why there are some reports on NiO in the literature that claim hole mobilities of more than $1\,\mathrm{cm^2\,V^{-1}s^{-1}}$, far outside the range typical for polaronic hopping transport [57–60]. In many of these works, the conductivity of the investigated films is in the range of 1×10^{-2} S cm^{-1} and higher, suggesting higher doping levels and thereby a stronger spatial overlap of the ZR wave functions than reported in this work. Also, sputtering at room temperature is typically used, leading to films with high structural and electronic disorder. The result is a broad band of V_{Ni} defect states. The main contribution of the conductivity can still be expected to come from hopping processes; however, a small part of the carriers occupy levels lying close enough in energy around ϵ_F that they can move in a very narrow band by almost activationless transport, similar to what was observed in our HT-NiO sample at low temperatures [Fig. 7(a)]. These carriers are able to generate a Hall voltage, while the hopping carriers are not. The hole densities extracted from these measurements are in the range of 10^{19} cm^{-3} or larger, but for the reason just explained, this is only a small subset of the overall hole population. Because the conductivity, on the other hand, is determined by both carrier types and therefore rather large, the calculated "Hall mobility" $\mu_{\mathrm{Hall}} = \frac{\sigma}{e p_{\mathrm{Hall}}}$ overestimates the value attributed to the hopping-determined conductivity.

IV. CONCLUSION

The temperature dependence of the dc and ac conductivity of intrinsically doped thin films can be consistently explained within the framework of polaronic interacceptor hopping conduction. This model is motivated by the perception of the nature of holes in doped NiO, which has been shown to be of strongly bound character (Zhang-Rice bound doublet). The ZR states are therefore situated deep inside the band gap, sufficiently well isolated from any extended valence band that charge transfer can only occur directly between the acceptors. The degree of structural and electronic disorder is of great importance for the conduction process. For samples of high disorder, Mott variable range hopping (VRH) can be applied well to model the behavior of σ_{dc} due to a large spread of the acceptor energies. VRH can be seen as a limiting case of the interacceptor hopping model for a broad distribution of acceptor states. In the case of low disorder, there is a clear change of the temperature behavior of σ_{dc} at about half the Debye temperature, $\frac{\theta_D}{2} \approx 200\,\mathrm{K}$, with multiphonon thermal activation above and phonon-assisted tunneling below that temperature, in accordance with the predictions of polaronic interacceptor hopping. Additionally, around and below this temperature the low-disorder sample exhibits a dielectric relaxation process in ε'' that is connected to the frequency cutoff of single-phonon-assisted hopping. The results from the VRH model and the parameters of this process give a localization length of the ZR holes of 0.62 nm and 0.85 nm, or about two lattice constants, for RT- and HT-grown NiO, respectively.

Furthermore, it is shown that disorder leads to the occurrence of strong interfacial polarization of mesoscopic regions in the film due to inhomogeneous conductivity (Maxwell-Wagner-Sillars polarization). This effect can produce a high apparent dielectric response under low-frequency ac electric fields. The current-voltage characteristics of NiO films sandwiched between Pt electrodes are non-ohmic but symmetrical,

with an increase of conductivity at higher dc electric fields that is observed at all temperatures. This could be attributed to a linear increase of the density of ZR states by hole injection. In these measurements, the temperature $\frac{\theta_D}{2}$ seems to be as critical as in the ac measurements, because it marks the onset of space-charge-limited conduction due to increasing carrier trapping time.

ACKNOWLEDGMENTS

This work was funded by the Deutsche Forschungsgemeinschaft (DFG) in the framework of the collaborative research centers "SFB 762: Functionality of Oxidic Interfaces" (Project No. B06) and "SFB/TRR 102: Polymers under Multiple Constraints" (Project No. B08).

[1] C. Wagner, Theorie der geordneten Mischphasen. III, Z. Phys. Chem. B **22**, 181 (1933).

[2] J. H. de Boer and E. J. W. Verwey, Semi-conductors with partially and with completely filled $_3d$-lattice bands, Proc. Phys. Soc. **49**, 59 (1937).

[3] R. R. Heikes and W. D. Johnston, Mechanism of conduction in Li-substituted transition metal oxides, J. Chem. Phys. **26**, 582 (1957).

[4] S. van Houten, Mechanical losses in Li-doped NiO semiconductors, J. Phys. Chem. Solids **23**, 1045 (1962).

[5] I. G. Austin, A. J. Springthorpe, B. A. Smith, and C. E. Turner, Electronic transport phenomena in single-crystal NiO and CoO, Proc. Phys. Soc. **90**, 157 (1967).

[6] A. Bosman and H. van Daal, Small-polaron versus band conduction in some transition-metal oxides, Adv. Phys. **19**, 1 (1970).

[7] D. Adler and J. Feinleib, Electrical and optical properties of narrow-band materials, Phys. Rev. B **2**, 3112 (1970).

[8] D. Snowden, H. Saltsburg, and J. Pereue, The frequency-dependent electrical conductivity of powders: Nickel oxide, J. Phys. Chem. Solids **25**, 1099 (1964).

[9] S. Kabashima and T. Kawakubo, High frequency conductivity of NiO, J. Phys. Soc. Jpn. **24**, 493 (1968).

[10] J. Aiken and A. Jordan, Electrical transport properties of single crystal nickel oxide, J. Phys. Chem. Solids **29**, 2153 (1968).

[11] M. A. Kolber and R. K. MacCrone, Bound-Polaron Hopping in NiO, Phys. Rev. Lett. **29**, 1457 (1972).

[12] P. Lunkenheimer, A. Loidl, C. R. Ottermann, and K. Bange, Correlated barrier hopping in NiO films, Phys. Rev. B **44**, 5927 (1991).

[13] G. E. Pike, AC conductivity of scandium oxide and a new hopping model for conductivity, Phys. Rev. B **6**, 1572 (1972).

[14] M. Nachman, L. N. Cojocaru, and L. V. Rîbco, Electrical properties of non-stoichiometric nickel oxide, Phys. Status Solidi B **8**, 773 (1965).

[15] A. Springthorpe, I. Austin, and B. Austin, Hopping conduction in $Li_xNi_{1-x}O$ crystals at low temperatures, Solid State Commun. **3**, 143 (1965).

[16] J. Bała, A. M. Oleś, and J. Zaanen, Zhang-Rice Localization, Quasiparticle Dispersions, and the Photoemission of NiO, Phys. Rev. Lett. **72**, 2600 (1994).

[17] F. C. Zhang and T. M. Rice, Effective Hamiltonian for the superconducting Cu oxides, Phys. Rev. B **37**, 3759 (1988).

[18] M. Taguchi, M. Matsunami, Y. Ishida, R. Eguchi, A. Chainani, Y. Takata, M. Yabashi, K. Tamasaku, Y. Nishino, T. Ishikawa *et al.*, Revisiting the Valence-Band and Core-Level Photoemission Spectra of NiO, Phys. Rev. Lett. **100**, 206401 (2008).

[19] R. Newman and R. M. Chrenko, Optical properties of nickel oxide, Phys. Rev. **114**, 1507 (1959).

[20] G. A. Sawatzky and J. W. Allen, Magnitude and Origin of the Band Gap in NiO, Phys. Rev. Lett. **53**, 2339 (1984).

[21] J. He, H. Lindström, A. Hagfeldt, and S.-E. Lindquist, Dye-sensitized nanostructured *p*-type nickel oxide film as a photocathode for a solar cell, J. Phys. Chem. B **103**, 8940 (1999).

[22] M. D. Irwin, D. B. Buchholz, A. W. Hains, R. P. H. Chang, and T. J. Marks, *p*-type semiconducting nickel oxide as an efficiency-enhancing anode interfacial layer in polymer bulk-heterojunction solar cells, Proc. Natl. Acad. Sci. USA **105**, 2783 (2008).

[23] S.-Y. Park, H.-R. Kim, Y.-J. Kang, D.-H. Kim, and J.-W. Kang, Organic solar cells employing magnetron sputtered *p*-type nickel oxide thin film as the anode buffer layer, Sol. Energy Mater. Sol. Cells **94**, 2332 (2010).

[24] S.-W. Park, J.-M. Choi, E. Kim, and S. Im, Inverted top-emitting organic light-emitting diodes using transparent conductive NiO electrode, Appl. Surf. Sci. **244**, 439 (2005).

[25] L. Y. Tang, X. L. Zhang, H. T. Dai, J. L. Zhao, S. G. Wang, and X. W. Sun, NiO as hole transport layers for all-inorganic quantum dot LEDs, in *Light-Emitting Diodes: Materials, Devices, and Applications for Solid State Lighting XVII*, edited by K. P. Streubel, H. Jeon, L.-W. Tu, and M. Strassburg (SPIE, San Francisco, California, 2013).

[26] S. Seo, M. J. Lee, D. C. Kim, S. E. Ahn, B.-H. Park, Y. S. Kim, I. K. Yoo, I. S. Byun, I. R. Hwang, S. H. Kim *et al.*, Electrode dependence of resistance switching in polycrystalline NiO films, Appl. Phys. Lett. **87**, 263507 (2005).

[27] S. I. Kim, J. H. Lee, Y. W. Chang, S. S. Hwang, and K.-H. Yoo, Reversible resistive switching behaviors in NiO nanowires, Appl. Phys. Lett. **93**, 033503 (2008).

[28] J.-Y. Jeng, K.-C. Chen, T.-Y. Chiang, P.-Y. Lin, T.-D. Tsai, Y.-C. Chang, T.-F. Guo, P. Chen, T.-C. Wen, and Y.-J. Hsu, Nickel oxide electrode interlayer in $CH_3NH_3PbI_3$ perovskite/PCBM planar-heterojunction hybrid solar cells, Adv. Mater. **26**, 4107 (2014).

[29] E. Avendaño, L. Berggren, G. Niklasson, C. Granqvist, and A. Azens, Electrochromic materials and devices: Brief survey and new data on optical absorption in tungsten oxide and nickel oxide films, Thin Solid Films **496**, 30 (2006).

[30] H. Huang, J. Tian, W. Zhang, Y. Gan, X. Tao, X. Xia, and J. Tu, Electrochromic properties of porous NiO thin film as a counter electrode for NiO/WO_3 complementary electrochromic window, Electrochim. Acta **56**, 4281 (2011).

[31] H. Moulki, D. H. Park, B.-K. Min, H. Kwon, S.-J. Hwang, J.-H. Choy, T. Toupance, G. Campet, and A. Rougier, Improved electrochromic performances of NiO based thin films by lithium addition: From single layers to devices, Electrochim. Acta **74**, 46 (2012).

[32] Y. Ren, W. K. Chim, L. Guo, H. Tanoto, J. Pan, and S. Y. Chiam, The coloration and degradation mechanisms of electrochromic nickel oxide, Sol. Energy Mater. Sol. Cells **116**, 83 (2013).

[33] S. Lany, J. Osorio-Guillén, and A. Zunger, Origins of the doping asymmetry in oxides: Hole doping in NiO versus electron doping in ZnO, Phys. Rev. B **75**, 241203(R) (2007).

[34] J. Y. Zhang, W. W. Li, R. L. Z. Hoye, J. L. MacManus-Driscoll, M. Budde, O. Bierwagen, L. Wang, Y. Du, M. J. Wahila, L. F. J. Piper, *et al.*, Electronic and transport properties of Li-doped NiO epitaxial thin films, J. Mater. Chem. C **6**, 2275 (2018).

[35] R. Karsthof, P. Räcke, H. von Wenckstern, and M. Grundmann, Semi-transparent NiO/ZnO UV photovoltaic cells, Phys. Status Solidi A **213**, 30 (2015).

[36] R. Karsthof, H. von Wenckstern, and M. Grundmann, Transparent JFETs based on NiO-ZnO heterojunctions, IEEE Trans. Electron Devices **62**, 3999 (2015).

[37] R. Karsthof, H. von Wenckstern, and M. Grundmann, Semitransparent ZnO-based UV-active solar cells: Analysis of electrical loss mechanisms, J. Vac. Sci. Technol., B: Nanotechnol. Microelectron.: Mater., Process., Meas., Phenom. **34**, 04J107 (2016).

[38] S. D. Nehate, A. Prakash, P. D. Mani, and K. B. Sundaram, Work function extraction of indium tin oxide films from MOSFET devices, ECS J. Solid State Sci. Technol. **7**, P87 (2018).

[39] H. B. Michaelson, The work function of the elements and its periodicity, J. Appl. Phys. **48**, 4729 (1977).

[40] H.-L. Chang, T. C. Lu, H. C. Kuo, and S. C. Wang, Effect of oxygen on characteristics of nickel oxide/indium tin oxide heterojunction diodes, J. Appl. Phys. **100**, 124503 (2006).

[41] A. Rose, Space-charge-limited currents in solids, Phys. Rev. **97**, 1538 (1955).

[42] J. Y. Son and Y.-H. Shin, Direct observation of conducting filaments on resistive switching of NiO thin films, Appl. Phys. Lett. **92**, 222106 (2008).

[43] D. Ielmini, F. Nardi, and C. Cagli, Physical models of size-dependent nanofilament formation and rupture in NiO resistive switching memories, Nanotechnology **22**, 254022 (2011).

[44] C. P. Liu, K. O. Egbo, C. Y. Ho, J. A. Zapien, W. Walukiewicz, and K. M. Yu, Stoichiometry controlled bipolar conductivity in nanocrystalline $Ni_xCd_{1-x}O_{1+\delta}$ thin films, Phys. Rev. Appl. **11**, 014019 (2019).

[45] I. Austin and N. Mott, Polarons in crystalline and non-crystalline materials, Adv. Phys. **18**, 41 (1969).

[46] H. Böttger and V. V. Bryksin, *Hopping Conduction in Solids* (Wiley-VCH, Weinheim, Germany, 1986).

[47] R. G. Allen, T. E. Stephenson, C. P. Stanford, and S. Bernstein, Slow neutron cross sections of gold, silver, indium, nickel, and nickel oxide, Phys. Rev. **96**, 1297 (1954).

[48] J. Schnakenberg, Polaronic impurity hopping conduction, Phys. Status Solidi B **28**, 623 (1968).

[49] N. Mott, Conduction in glasses containing transition metal ions, J. Non-Cryst. Solids **1**, 1 (1968).

[50] N. F. Mott, Conduction in non-crystalline systems, Philos. Mag. **17**, 1259 (1968).

[51] F. Kremer and A. Loidl, editors, *The Scaling of Relaxation Processes* (Springer International Publishing, Basel, Switzerland, 2018).

[52] F. Kremer and A. Schönhals, *Broadband Dielectric Spectroscopy* (Springer, Berlin, 2002).

[53] M. Samet, G. Boiteux, G. Seytre, A. Kallel, and A. Serghei, Interfacial polarization in composite materials with spherical fillers: Characteristic frequencies and scaling laws, Colloid Polym. Sci. **292**, 1977 (2014).

[54] J. C. Dyre and T. B. Schrøder, Universality of AC conduction in disordered solids, Rev. Mod. Phys. **72**, 873 (2000).

[55] P. J. Gielisse, J. N. Plendl, L. C. Mansur, R. Marshall, S. S. Mitra, R. Mykolajewycz, and A. Smakula, Infrared properties of NiO and CoO and their mixed crystals, J. Appl. Phys. **36**, 2446 (1965).

[56] A. Long, Frequency-dependent loss in amorphous semiconductors, Adv. Phys. **31**, 553 (1982).

[57] H. Sato, T. Minami, S. Takata, and T. Yamada, Transparent conducting *p*-type NiO thin films prepared by magnetron sputtering, Thin Solid Films **236**, 27 (1993).

[58] R. Molaei, R. Bayati, and J. Narayan, Crystallographic characteristics and *p*-type to *n*-type transition in epitaxial NiO thin film, Crystal Growth and Design **13**, 5459 (2013).

[59] Y. Chen, Y. Sun, X. Dai, B. Zhang, Z. Ye, M. Wang, and H. Wu, Tunable electrical properties of NiO thin films and *p*-type thin-film transistors, Thin Solid Films **592**, 195 (2015).

[60] M. Tyagi, M. Tomar, and V. Gupta, Trap assisted space charge conduction in *p*-NiO/*n*-ZnO heterojunction diode, Mater. Res. Bull. **66**, 123 (2015).